An OpenFOAM-Integrated Numerical Solver for Electroconvective Flow

Duc-Anh Van, Hoang-Thang Do, Van-Sang Pham*

Hanoi University of Science and Technology, Hanoi, Vietnam
*Email: sang.phamvan@hust.edu.vn

Abstract

In this work, we developed a numerical solver, integrated it into the OpenFOAM platform, for modeling electroconvective flow. The solver deals with the system of Poisson-Nernst-Planck-Navier-Stokes equations. The finite volume schemes functioned in OpenFOAM were used for discretisation of the Poisson-Nernst-Planck equations. The Newton method was employed to solve the nonlinear Poisson-Nernst-Planck equations in a coupled manner. The validation shows the high accuracy of our solver. It is used to investigate ion conduction in the electrodialysis cell. The simulation results have allowed examining the flow's profile, ion distribution in different regimes of the system. Especially, the mechanisms behind the vortex formation in the channel can be explained by these results. This solver developed on OpenFoam open-source code provides the research community with a valuable tool for the study of electrochemical problems.

Keywords: Poisson-Nernst-Planck-Navier-Stokes, electrokinetics, ion concentration polarization.

1. Introduction

Transportation of charged species can be found in many areas such as water desalination, microfluidic, biomedical, fuel cells [1], etc., and the mechanisms which cause transportation include drift, diffusion, and convection of charged species in the flow.

The movements of charged species in biological systems are theoretically described by the Nernst-Planck model. In this model, the transportation of charged species is governed by a system of the coupled Poisson-Nernst-Planck equations which describe it through mechanisms of diffusion, electromigration, and convection. The Poisson-Nernst-Planck (PNP) model is applied widely in modeling dilute solutions in chemistry, biology, and many other engineering sciences.

However, PNP equations are highly nonlinear systems, so there are some difficulties solving them numerically. Especially, in the electrical double layer (EDL) which contains strong accumulation with rapidly electric potential changing of the permselective membrane, some of them are (i) the stiff nonlinear coupling and (ii) the rapidly electrical body force field change. Normally, with a lower nonlinear system like Navier-Stokes (NS), we solve it by using the sequential method, Piso and Simple, for example. However, if we apply this method for PNP, the number of iterations required is huge. In order to avoid this problem, we developed a new solver in OpenFoam platform for solving the sets of PNP and NS equation with a couple of methods. The velocity from the previous iteration or initial condition will be used to calculate the potential and concentration from PNP

equations at the same time. Then the obtained electric body force will be put into the NS equations. After the velocity field has been calculated, it is substituted into the PNP equations. The process is repeated until convergence is reached. Due to the conservative of PNP and NS equations, the finite volume method is used to discrete them. This method is also the foundation of OpenFoam. In addition, the ease in meshing procedure and coupling with NS and PNP equations lead us to a new solver in OpenFoam.

The solver was validated and used for simulating electrokinetic flow in several electrochemical systems such as electrodialysis cell, ion concentration polarization phenomenon near ion exchange membrane. Obtained simulation results are in good agreement with the experiment, indicating that the solver can be a valuable tool for the design and optimization of electrochemical devices.

2. Mathematical Model

2.1. Mathematical Model

In the system, ion transportation is governed by the Nernst-Plank (1) and (2); the relationship between electric potential field and ion concentrations is demonstrated by Poisson (3) and (4); and the fluid motion is described by the Navier-Stokes (5) and (6). The dimensionless form of these equations is as follow:

$$\frac{1}{\widetilde{\lambda_D}}\frac{\partial \widetilde{C_\pm}}{\partial \tilde{t}} = -\widetilde{\nabla} \cdot \tilde{J}_\pm \qquad (1)$$

$$\tilde{J}_\pm = -\widetilde{D}_\pm(\widetilde{\nabla}\tilde{C}_\pm + Z_\pm \tilde{C}_\pm \widetilde{\nabla}\tilde{\Phi}) + Pe\widetilde{U}\tilde{C}_\pm \qquad (2)$$

$$\tilde{\lambda}_D^2 \tilde{\nabla} \cdot (\tilde{\nabla}\tilde{\Phi}) = -\tilde{\rho}_e \qquad (3)$$

$$\tilde{\rho}_e = Z_+ \tilde{C}_+ + Z_- \tilde{C}_- \qquad (4)$$

$$\frac{1}{Sc} \frac{1}{\tilde{\lambda}_D} \frac{\partial \tilde{U}}{\partial \tilde{t}} = -\tilde{\nabla}\tilde{P} + \tilde{\nabla}^2 \tilde{U} - R(\tilde{U} \cdot \tilde{\nabla})\tilde{U} \qquad (5)$$

$$- \frac{1}{\tilde{\lambda}_D^2} \tilde{\rho}_e \tilde{\nabla}\tilde{\Phi}$$

$$\tilde{\nabla} \cdot \tilde{U} = 0 \qquad (6)$$

where $\tilde{t}$, $\widetilde{C_\pm}$, $\tilde{\Phi}$, $\tilde{U}$, $\tilde{P}$ denote the dimensionless time, concentration of cations (+) and anions (-), electric potential, vector of fluid velocity, and pressure, respectively. These quantities are normalized by the corresponding reference values of time, ionic concentration, electric potential, velocity, and pressure, respectively as follow:

$$\tau_0 = \frac{l_0^2}{D_0}; C_0 = C_{bulk}; \Phi_0 = \frac{k_B T}{Ze};$$

$$U_0 = \frac{\epsilon \Phi_0}{\eta l_0}; P_0 = \frac{\eta U_0}{l_0}$$

where C_0 is the concentration scale, l_0 is the characteristic length scale, D_0 is the average diffusivity, k_B is the Boltzmann constant, T is the absolute temperature, e is the elementary charge, $Z = |Z_\pm|$ is ion valence, η is the dynamic viscosity of the solution, and ϵ is the permitivity of the solvent. Parameters $\tilde{D}_\pm = \frac{D_\pm}{D_o}$, $\tilde{\lambda}_D = \frac{\lambda_D}{l_o}$, and $\tilde{\rho}_e = \frac{\rho_e}{C_o}$ are dimensionless diffusion coefficient, the Debye length, and the space charge, respectively. $Pe = U_0 l_0 / D_0$, $Sc = \eta / \rho_m D_0$, and $R = U_0 l_0 \rho_m / \eta$ are the Péclet number, the Schmidt number, and the Reynolds number, respectively [2].

In this study, $\tilde{\lambda}_D = 0.0005$, corresponds to the characteristic length $l_0 = 20\mu m$, bulk concentration $C_0 = 1\ mM(NaCl)$, and the absolute temperature $T = 300K$. Other parameters used in the simulation include the diffusivities $D_+ = 1.33 * 10^{-9}\ m^2 s^{-1}$, $D_- = 2.03 * 10^{-9}\ m^2 s^{-1}$, $\tau_0 = 2.381e^{-1}(s)$, $Pe = 0.28$, $U_0 = 2.367e^{-5}(m/s)$, $\Phi_0 = 2.585e^{-2}(vol)$, $V_0 = 0.25852\ V$.

2.2. Numerical Method

The finite volume method, a locally conservative method, is used for the discretization of the equations. The solution domain is subdivided into a finite number of control volumes, then the governing equations are integrated over the control volumes, the resultant volume integrals are then converted to surface integrals using Gauss' theorem. The face quantities of the surface integrals are evaluated in terms of the unknowns at the centroid of the control volume and its neiboughring cells, as denoted by P and N, respectively, in Fig. 1:
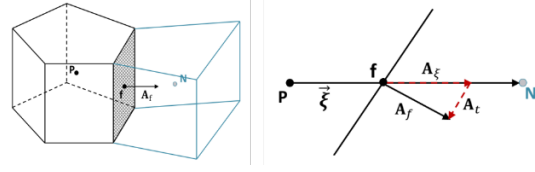

Fig. 1. A typical control volume is denoted by P.

Neighbor of the control volume is denoted N. The face shared by P and N is denoted by f having area vector $\mathbf{A}_f$. Area vector $\mathbf{A}_f$ is decomposed into two components $\mathbf{A}_f, \mathbf{A}_t$.

To obtain the discretization for the Nernst-Planck equation, we integrate (1) over a control volume, and use the Gauss'theorem to yield:

$$\int \partial_t C_i dV = -\sum J_{if} \cdot A_f \qquad (7)$$

For the temporal discretization, we use an implicit, second order accuracy scheme:

$$\int_{V_P} \frac{\partial C_i}{\partial t} dV = \frac{3V_P}{2\Delta t} C_{iP}^n + \frac{V_P}{2\Delta t}(-4C_{iP}^{n-1} \qquad (8)$$
$$+ C_{iP}^{n-2})$$

where C_{iP}^{n-1} and C_{iP}^{n-2} are values at the previous *n-1* and *n-2* steps, respectively.

The ion fluxes passing through face f have the following form:

$$J_i = -D_i(\nabla C_i + u_i z_i F C_i \nabla \phi) + C_i U \qquad (9)$$

The diffusion, migration, and convection terms presented in the ion flux are discretized using central differencing and interpolating schemes.

The discretization for the Poisson-Nernst-Planck equations generates a system of nonlinear equations. There are a number of methods that can be used to solve the system, such as Newton-Raphson method, secant method, and Brent method. In this study, we make use the Newton-Raphson method because of its fast convergence [3]. In the following part, we briefly introduce the Newton-Raphson method for a system of nonlinear equations.

In the next sections, we will derive expressions for the entries of the Jacobian matrix and the function.

Consider three functions *F1*, *F2*, *F3* corresponding to three equations of PNP equation. The value of the functions is determined by variable values at the control volume centroid and its neighboring control volumes at the current time step.

$$F1 = \frac{1}{\varepsilon} \frac{3V_P}{2\Delta t} C_{1P}^n + \frac{1}{\varepsilon} \frac{V_P}{2\Delta t}(-4C_{1P}^{n-1} + C_{1P}^{n-2}) \qquad (10)$$
$$+ \sum_{f=1}^{n_f} (-D_1(\nabla C_1 + C_1 \nabla \phi)$$
$$+ PeC_1 U)_f \cdot \mathbf{A}_f = 0$$

$$F2 = \frac{1}{\varepsilon}\frac{3V_P}{2\Delta t}C_{2P}^n + \frac{1}{\varepsilon}\frac{V_P}{2\Delta t}\left(-4C_{2P}^{n-1} + C_{2P}^{n-2}\right) \tag{11}$$
$$+ \sum_{f=1}^{n_f}(-D_2(\nabla C_2 + C_2\nabla\phi)$$
$$+ PeC_2U)_f \cdot \mathbf{A}_f = 0$$

$$F3 = \sum_{f=1}^{n_f}(\nabla\phi)_f \cdot \mathbf{A}_f = \frac{-1}{\varepsilon^2}\sum_{f=1}^{n_f}Z_iC_i V_P = 0 \tag{12}$$

Entries of the Jacobian matrix are defined by differentiating the functions with respect to the variables at the current control volume and its neighbors.

Matrix entries corresponding to the ion concentration and electric potential in the Nernst-Planck equation for ion i written at control volume P are calculated using the following formulas:

$$J(C_i)_P^{Nerst-Plank} = \sum_{f=1}^{n_f}\frac{\partial J_{if}}{\partial C_{ip}} \tag{13}$$
$$= -\frac{1}{|\xi|}\frac{\mathbf{A}_f.\mathbf{A}_f}{\mathbf{A}_f.\mathbf{i}_\xi}$$
$$+ z_i(1$$
$$- \gamma)\left(\frac{\phi_N - \phi_P}{|\xi|}\right)\frac{\mathbf{A}_f.\mathbf{A}_f}{\mathbf{A}_f.\mathbf{i}_\xi}$$
$$- PeU_f.\mathbf{A}_f(1 - \gamma)$$

$$J(\phi_i)_P^{Nerst-Plank} = \sum_{f=1}^{n_f}\frac{\partial J_{if}}{\partial \phi_p} \tag{14}$$
$$= -\frac{1}{|\xi|}z_i(\gamma C_{iP} + (1$$
$$- \gamma)C_{iN})\frac{\mathbf{A}_f.\mathbf{A}_f}{\mathbf{A}_f.\mathbf{i}_\xi}$$

$$J(C_i)_P^{Poisson} = \frac{1}{m}z_i \tag{15}$$

$$J(C_i)_P^{Poisson} = -\varepsilon^2 \sum_{f=1}^{n_f}\frac{1}{|\xi|}\frac{\mathbf{A}_f.\mathbf{A}_f}{\mathbf{A}_f.\mathbf{i}_\xi} \tag{16}$$

The discretized block coupled system of equations is obtained and have the general form:

$$A_C X_C + \sum A_{NB} X_{NB} = B_C \tag{17}$$

where X_C, X_{NB}, B_C denote the solution vector at the cell center and its neighbour cells, the source term equivalent to the function value F, respectively.

$$X_C = \begin{pmatrix} \Delta C_{1C} \\ \Delta C_{2C} \\ \Delta \phi_C \end{pmatrix}, X_{NB} = \begin{pmatrix} \Delta C_{1NB} \\ \Delta C_{2NB} \\ \Delta \phi_{NB} \end{pmatrix}, B_C = \tag{18}$$
$$\begin{pmatrix} F_1 \\ F_2 \\ F_3 \end{pmatrix}$$

A_C, A_{NB} denote the diagonal and off-diagonal elements of the block matrix, respectively.

$$A_C = \begin{pmatrix} a_C^{C_1 C_1} & a_C^{C_1 C_2} & a_C^{C_1 \phi} \\ a_C^{C_2 C_1} & a_C^{C_2 C_2} & a_C^{C_2 \phi} \\ a_C^{\phi C_1} & a_C^{\phi C_2} & a_C^{\phi \phi} \end{pmatrix} \tag{19}$$

$$A_{NB} = \begin{pmatrix} a_{NB}^{C_1 C_1} & a_{NB}^{C_1 C_2} & a_{NB}^{C_1 \phi} \\ a_{NB}^{C_2 C_1} & a_{NB}^{C_2 C_2} & a_{NB}^{C_2 \phi} \\ a_{NB}^{\phi C_1} & a_{NB}^{\phi C_2} & a_{NB}^{\phi \phi} \end{pmatrix}$$

Assemble (18), (19) into (17), we have full form of the system of equations

$$\begin{pmatrix} a_C^{C_1 C_1} & a_C^{C_1 C_2} & a_C^{C_1 \phi} \\ a_C^{C_2 C_1} & a_C^{C_2 C_2} & a_C^{C_2 \phi} \\ a_C^{\phi C_1} & a_C^{\phi C_2} & a_C^{\phi \phi} \end{pmatrix}\begin{pmatrix} \Delta C_{1C} \\ \Delta C_{2C} \\ \Delta \phi_C \end{pmatrix} \tag{20}$$
$$+ \sum \begin{pmatrix} a_{NB}^{C_1 C_1} & a_{NB}^{C_1 C_2} & a_{NB}^{C_1 \phi} \\ a_{NB}^{C_2 C_1} & a_{NB}^{C_2 C_2} & a_{NB}^{C_2 \phi} \\ a_{NB}^{\phi C_1} & a_{NB}^{\phi C_2} & a_{NB}^{\phi \phi} \end{pmatrix}\begin{pmatrix} \Delta C_{1NB} \\ \Delta C_{2NB} \\ \Delta \phi_{NB} \end{pmatrix}$$
$$= \begin{pmatrix} F_1 \\ F_2 \\ F_3 \end{pmatrix}$$

The coupled algorithm involves the following steps:

1. Initialize variables $(X_k = 0)$

2. Assemble Jacobian Matrix J^k with entries calculated from discretized equations and evaluate the function value F_k.

3. Solve the system of linearized equations to obtain a new approximation of the solution:

$$J^k(X^k)\Delta X^{k+1} = F^k(X^k) \tag{21}$$
$$X^{k+1} = X^k + \Delta X^{k+1}$$

4. Check convergence and return to step 1 if not satisfied:

$$\|\Delta X^{k+1}\| < \epsilon \tag{22}$$

Solving the PNP equations using Newton-Raphson method is an iterative process. It requires to recompute the Jacobian matrix and function value iteratively. To resolve the rapid variations of the ion concentrations and electric potential near charged surfaces, the mesh at the membrane/solution interface needed to be refined toward the membrane surfaces. To avoid solving the large system of linear equations, we solve the PNP and NS equations alternatively [4]. Starting with a velocity field from the previous iteration or initial condition, the potential and concentrations are simultaneously solved from the PNP equations. Then, electric body force is calculated and substituted into the NS equations. The velocity field obtained by solving the NS equations is

substituted back into the PNP equations. The process is repeated until convergence is reached.

The numerical solver was validated by comparing the numerical solution to the analytical solution and solution published in the papers [5,6] of electric potential on a solid surface interfacing with an electrolyte solution. The potential can be calculated using the well-known Grahame equation:

$$\phi_{surface} \quad (23)$$
$$= \frac{2k_B T}{e} \sinh^{-1}\left(\frac{\sigma}{\frac{(8\epsilon\epsilon_0 k_B T n_{KCl})^1}{2}}\right)$$

where σ (C / m^2) is the charge density on the solid surface.

To examine the effect of mesh nonorthogonality on the simulation result, we consider two mesh types including an orthogonal mesh (consisting of rectangular control volume), a non-orthogonal mesh (consisting of triangular control volumes). Parameters used in the simulation include the bulk concentration with different values ($0.1mM, 1mM, 10mM$), surface charge, temperature $T = 300K$, the diffusivities.

The numerical and exact solutions for the surface potential at different bulk concentrations are presented in Table 1. From the results, we can see a good agreement between the exact solution and the numerical solution for both orthogonal and non-orthogonal meshes. This agreement demonstrates the high accuracy of our numerical solution.

Table 1. The computed surface potential and ion concentration in comparison with published data.

C_{bulk}	$\phi(mV)$	$\phi(mV)$	$\phi(mV)$	$\phi(mV)$	$\phi(mV)$
	Analytical	Orthogonal	Non orthogonal	Marthr and Murthy [5]	Daijuji *et al* [6]
0.1	-39.5	-39.52	-39.5	-39.58	-39.5
1	-13.5	-13.6	-13.62	-13.36	-13.7
10	-4.34	-4.35	-4.35	-4.42	-4.42

3. Results and Discussion

We apply our numerical solver by simulating an electrodialysis cell that existed in electrodialysis desalination system [7-9]. The electrodialysis cell is a microchannel with a size of 20 x 10 x 60 um. The microchannel is constructed with an anion-exchange membrane (AEM) on top and a cation-exchange membrane (CEM) at the bottom. Salt solution is pumped into an end (inlet), due to the electric field remaining across the membranes, which extracts salt gradually when the solution flows along the channel.

The desalted solution is then obtained at the other end of the channel (outlet). A sketch of the electrodialysis cell is provided in Fig. 2.
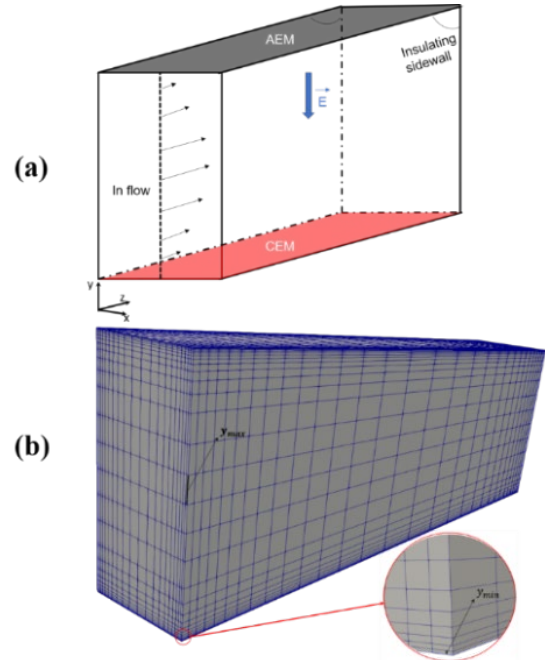

Fig. 2. (a) Sketch of a electrodialysis cell. On top and bottom are cation exchange membranes AEM (top) and CEM (bottom). (b) The electrodialysis cell simulation model.

The purpose of the simulation is to investigate the electrokinetic flow in the microchannel, particularly, to observe the electroconvective instability in an electrodialysis cell of which the permselective membranes interface with a pressure-driven electrolyte flow. To conduct the simulation, the following boundary conditions are enforced on the microchannel boundaries. On the AEM and CEM boundaries, the common boundary conditions for ion concentrations at ion-exchange membrane are employed: fixed value for concentration of counter ions ($C_m = C_0$), and no-flux condition for co-ions [1,4,9,11]. Flow is generated by velocity at the inlet and fixed value pressure at the outlet. The ion concentrations at the channel entrance are fixed at the bulk concentration ($C_m = C_0$). No-slip boundary condition is assumed at the membrane surfaces.

The control parameter in our simulation is the bias voltage applied between the membranes. Different bias voltages are enforced by changing the potential on the CEM while keeping that on the AEM at zero.

The mesh of 18000 cells refining the region near membrane is used (Fig. 2a). The maximum of cell size in y direction $y_{max} = 0.1l_0$ placing in the center region while the minimum is $y_{min} = 0.00145l_0$ placing near

membranes ($l_0=2^{-5}$ is the length scale). M4800 Dell workstation computer with Intel i7, 2.4Gh, processor, and 8 Gb of Ram is used. The average time solution for each voltage in three regimes is 14,52s, 30.71s, 293.15s respectively.

In the following sections, the results for voltage-current response, development of electroconvective flow in the channel, and impact of the flow on the ion distributions will be presented and discussed.

3.1. Voltage Current Response of the Electrochemical System

The mechanism of operation electrodialysis system manifests on a current-voltage curve (I-V curve). To obtain it, the ion transport processing on the ion exchange membrane was simulated under various applied voltages. The integral of cation and anion over the membrane area is used to calculate the current through this system. The simulation result is depicted in Fig. 3, which shows three regimes of ICP system operation including Ohmic, limiting, and over-limiting. In the Ohmic regime, when applying a small bias voltage between 0 and 10 V_0, ion is conducted through the membrane by the electric field. These results indicate the decrease in ion concentrations near the membrane and the increase in current. However, as the applied voltage is higher than about 10 V_0, the concentration of ion near the membrane surface approaches zero. The vanishing of ion near membrane makes modestly the increase in the current when the applied voltage increases from 10 V_0 to 24 V_0. Above 24 V_0, however, the current rising again indicated the appearance of over-limiting phenomena in the system.
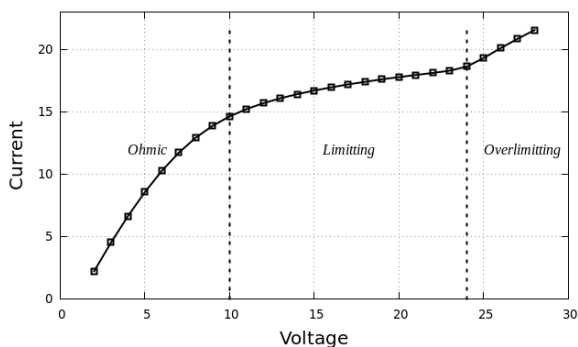

Fig. 3. The current-voltage curve of the electrodialysis cell.

The simulated results about three different regime operations are in good agreement with the previous experimental and theoretical studies on the ICP system [10,12].

3.2. Development of Electroconvective Flow Near Membanre Surface

The electrical force field in the system exerts force on space charge ($\tilde{\rho}_e$) distributed in the microchannel between two membranes. In this section, we examine its effect on the profile of flow in the microchannel.

The modeling result of the velocity flow inside the channel is depicted in Fig. 4. As we can observe, in Ohmic and limiting regime, the flow is almost unchanged by the effect of the body electric force field. In over-limiting regime, however, its profile was very different with the forming of helical vortices in the channel. The profile of flow might be explained from the simulation resulting. In Ohmic and limiting regimes, due to the neutrality of most of the volume in the system, the force field has a weak value in such location. Except for the layer near the exchange ion membrane where the ionic polarization occurs, the force field has a higher value. This body force, however, acts in a direction normal to the membrane just making an increase of the pressure in small volume near membrane (Fig. 5). As the applied voltage continues to increase (over-limiting regime), a space charge layer near the membrane surface is expanded. The electric body force begins to influence significantly on electroconvective flow here (Fig. 4c). This unstable layer led to the changing of flow configuration which features a couple vortex.

3.3. Impact of Electroconvective Low on Ions Distribution

The major factor in effective desalination is ion distribution in micro-channel. The impact of flow on it will be examined in this section.

The simulation of ion distribution is illustrated in Fig. 6. The concentration contour indicates that in Ohmic and limiting regimes the ion isometric surface is nearly laminar but does not uniform in over-limiting regime. To clarify this phenomenon, we show the simulated ion concentration on the symmetry plane of the system and at the outlet (Fig. 7). In *x* direction, there is little concentration variation in Ohmic and limiting regimes. However, the concentration profile in the width direction shows the electrokinetic instability of the system in over-limiting regime. This may indicate that the flow configuration on channel crosses section (Fig. 8). The ions in the middle region near selective membrane are swept by the stream of the combination of two symmetrical vortices, causing this layer thickness to increase significantly here. In contrast, on either side of the cross section, the ions are pushed through membrane, leading to the thickness reduction.
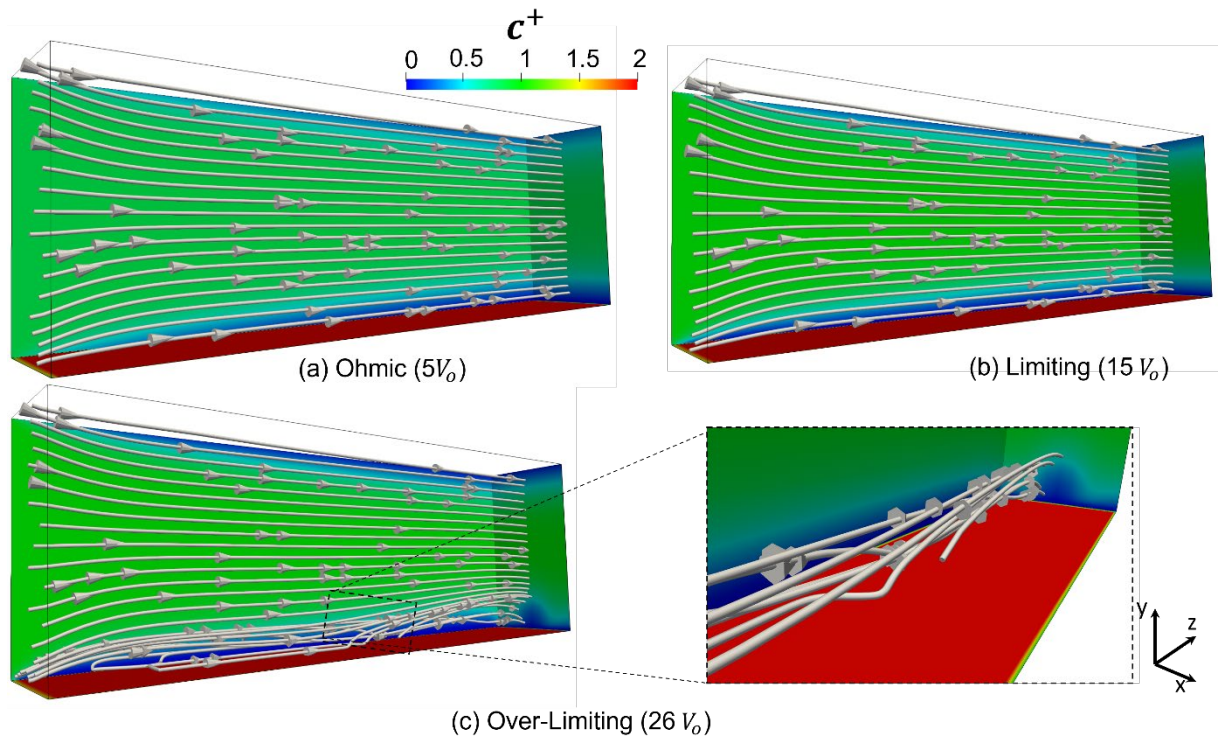
Fig. 4. Development of electroconvective flow near membrane surface in three regimes: (a) Ohmic, (b) limiting, (c) over-limiting
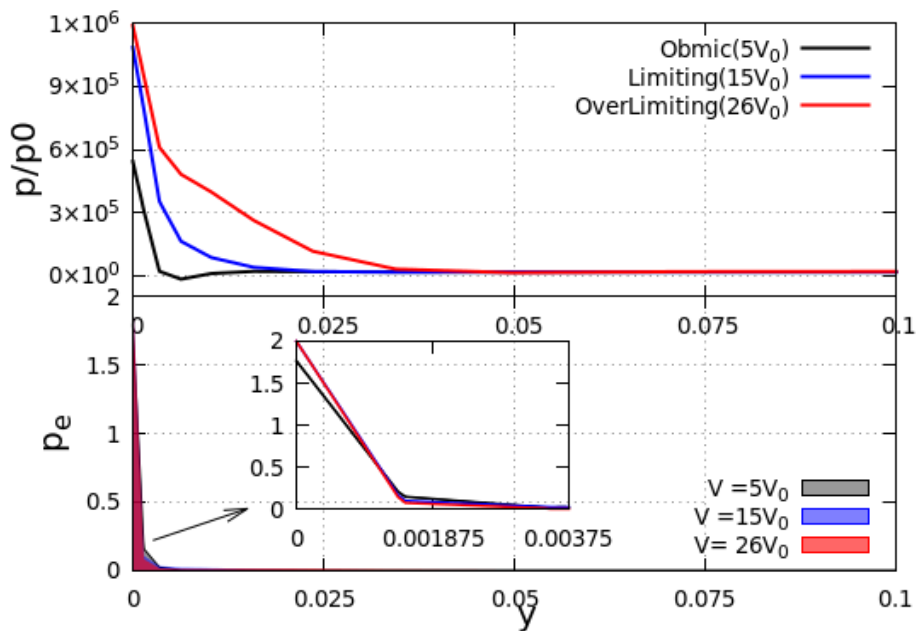

Fig. 5. Profile of space chare (p_e) near CEM membrane in the Ohmic ($V = 5V_0$), limiting ($V = 15V_0$) and over-limitting ($V = 26V_0$). Due to the development of an extended space charge layer, the pressure can be changed.
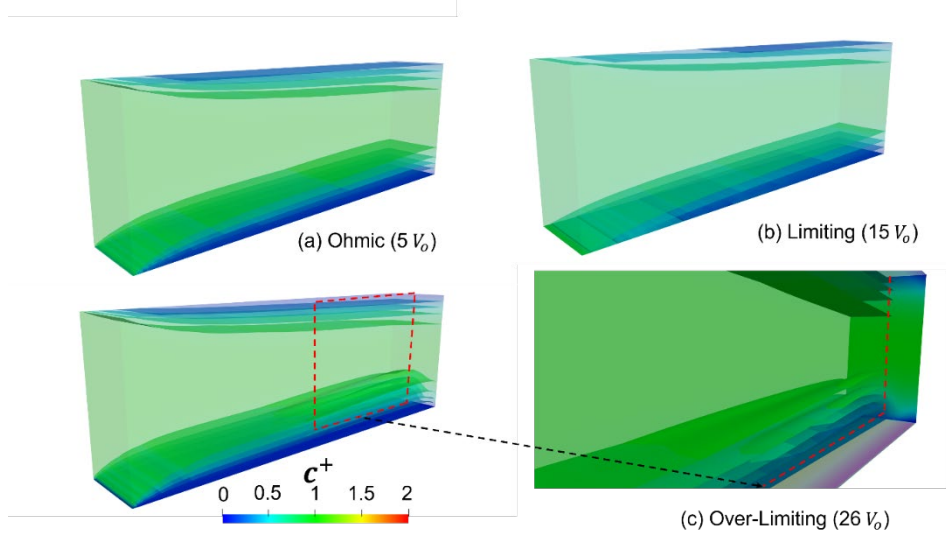
Fig. 6. Simulation result for ions concentration in three regimes: (a) Ohmic, (b) limiting, (c) over-limiting.
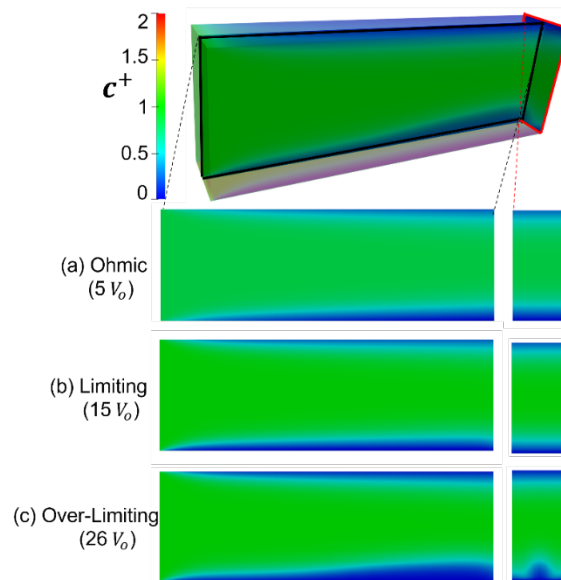

Fig. 7. Simulation results for concentration on the symmetry plane and at the outlet are shown in different regimes: (a) Ohmic, (b) limiting, (c) over-limiting.
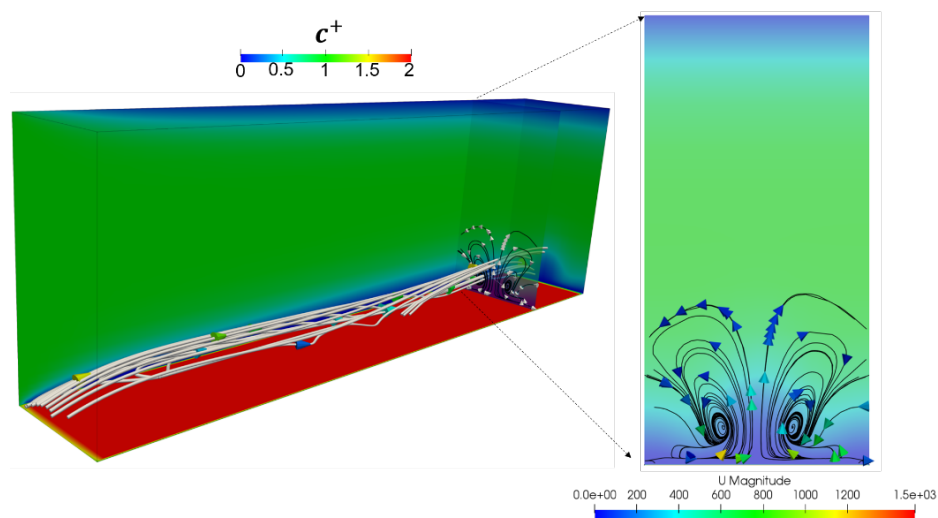

Fig. 8. Flow configuration on the channel cross section in over-limiting regime.

4. Conclusion

In this work, an OpenFoam integrated numerical solver for PNP-NS equation was developed. The obtained results show the high accuracy of the solver. It is applied in studying ion transport with different regimes in electrodialysis cell. The good results achieved enable us to fully explain, analyze the formation of electroconvective flow in electrodialysis cell. The numerical solver developed in this work provides a favorable open tool for OpenFoam research teams to investigate phenomena in the electrochemical field.

Acknowledgment

References

[1] V.-B. Nguyen and V.-S. Pham, Study and modeling DNA-preconcentration microfluidic device, J. Sci. Technol, vol. 143, no. 1, pp. 1–6. 2020.

[2] V. S. Pham, Z. Li, K. M. Lim, J. K. White, and J. Han, Direct numerical simulation of electroconvective instability and hysteretic current-voltage response of a permselective membrane, Phys. Rev. E - Stat. Nonlinear, Soft Matter Phys., vol. 86, no. 4. 2012. https://doi.org/10.1103/PhysRevE.86.046310.

[3] R. J. Hunter, Zeta Potential In Colloid Science, San Diego: Academic press Inc, 1981.

[4] I. Rubinstein and B. Zaltzman, Electro-osmotically induced convection at a permselective membrane, Phys. Rev. E - Stat. Physics, Plasmas, Fluids, Relat. Interdiscip. Top, vol. 62, no. 2, pp. 2238–2251. 2000. https://doi.org/10.1103/PhysRevE.62.2238.

[5] S. R. Mathur and J. Y. Murthy, A multigrid method for the Poisson – Nernst – Planck equations, Int. J. Heat Mass Transf, vol. 52, no. 17–18, pp. 4031–4039. 2009. https://doi.org/10.1016/j.ijheatmasstransfer.2009.03.040.

[6] H. Daiguji, P. Yang, and A. Majumdar, Ion transport in nanofluidic channels, Nano Letters, 2004 4 (1), pp. 137-142. https://doi.org/10.1021/nl0348185

[7] H. J. Kwon, B. Kim, G. Lim, and J. Han, A multiscale-pore ion exchange membrane for better energy efficiency, J. Mater. Chem. A, vol. 6, no. 17, pp. 7714–7723. 2018. https://doi.org/10.1039/c7ta10570c.

[8] J. Yoon, V. Q. Do, V. S. Pham, and J. Han, Return flow ion concentration polarization desalination: A new way to enhance electromembrane desalination, Water Res, vol. 159, pp. 501–510. 2019 https://doi.org/10.1016/j.watres.2019.05.042.

[9] V. S. Pham, Z. Li, K. M. Lim, J. K. White, and J. Han, Direct numerical simulation of electroconvective instability and hysteretic current-voltage response of a permselective membrane, Phys. Rev. E-Stat. Nonlinear, Soft Matter Phys, vol. 86, no. 4, pp. 1–11. 2012. https://doi.org/10.1103/PhysRevE.86.046310.

[10] S. V. Pham, H. Kwon, B. Kim, J. K. White, G. Lim, and J. Han, Helical vortex formation in three-dimensional electrochemical systems with ion-selective membranes, Phys. Rev. E, vol. 93, no. 3. 2016. https://doi.org/10.1103/PhysRevE.93.033114.

[11] C. L. Druzgalski, M. B. Andersen, and A. Mani, Direct numerical simulation of electroconvective instability and hydrodynamic chaos near an ion-selective surface, Phys. Fluids, vol. 25, no. 11. 2013. https://doi.org/10.1063/1.4818995.

[12] H. C. Chang and G. Yossifon, Understanding electrokinetics at the nanoscale: A perspective, Biomicrofluidics, vol. 3, no. 1, pp. 1–16. 2009. https://doi.org/10.1063/1.305604